Applied Catalysis B: Environmental 197 (2016) 271–279

Contents lists available at ScienceDirect

Applied Catalysis B: Environmental

journal homepage: www.elsevier.com/locate/apcatb

Phosphorus poisoning during wet oxidation of methane over Pd@CeO_2/graphite model catalysts

Matteo Monai[a], Tiziano Montini[a], Michele Melchionna[a], Tomáš Duchoň[b], Peter Kúš[b], Nataliya Tsud[b], Kevin C. Prince[c,d], Vladimir Matolin[b], Raymond J. Gorte[e], Paolo Fornasiero[a,*]

[a] Department of Chemical and Pharmaceutical Sciences, ICCOM-CNR URT Trieste, Consortium INSTM Trieste Research Unit, University of Trieste, via L. Giorgieri 1, 34127 Trieste, Italy
[b] Charles University in Prague, Faculty of Mathematics and Physics, Department of Surface and Plasma Science, V Holešovičkách 2, 18000 Prague, Czech Republic
[c] Elettra-Sincrotrone Trieste SCpA, Strada Statale 14, km 163.5, 34149 Basovizza, Trieste, Italy
[d] IOM, Strada Statale 14, km 163.5, 34149 Basovizza, Trieste, Italy
[e] Department of Chemical and Biomolecular Engineering, University of Pennsylvania, 311A Towne Building, 220 South 33rd Street, Philadelphia, USA

ARTICLE INFO

Article history:
Received 11 August 2015
Received in revised form
28 September 2015
Accepted 1 October 2015
Available online 9 October 2015

Keywords:
Phosphorus
Catalytic converters
Methane
Palladium
Ceria

ABSTRACT

The influence of phosphorus and water on methane catalytic combustion was studied over Pd@CeO_2 model catalysts supported on graphite, designed to be suitable for X-ray Photoelectron Spectroscopy/Synchrotron Radiation Photoelectron Spectroscopy (XPS/SRPES) analysis. In the absence of P, the catalyst was active for the methane oxidation reaction, although introduction of 15% H_2O to the reaction mixture did cause reversible deactivation. In the presence of P, both thermal and chemical aging treatments resulted in partial loss of activity due to morphological transformation of the catalyst, as revealed by Scanning Electron Microscopy (SEM) and Atomic Force Microscopy (AFM) analysis. At 600 °C the combined presence of PO_4^{3-} and water vapor caused a rapid, irreversible deactivation of the catalyst. XPS/SRPES analysis, combined with *operando* X-ray Absorption Near Edge Structure (XANES) and AFM measurements, indicated that water induces severe aggregation of CeO_2 nanoparticles, exposure of $CePO_4$ on the outer layer of the aggregates and incorporation of the catalytic-active Pd nanoparticles into the bulk. This demonstrates a temperature-activated process for P-poisoning of oxidation catalysts in which water vapor plays a crucial role.

1. Introduction

Palladium-based catalysts are the most active materials for oxidation of methane at low temperatures [1,2], and especially high activity can be achieved when the Pd is in the presence of reducible promoters such as ceria (CeO_2) [3–5]. The promoter helps stabilize PdO (the most active phase) against thermal decomposition to less active Pd, improving the catalytic performance by activation and spillover of oxygen from the promoter to the Pd phase [2,4,5]. Indeed, recent work has shown that the activity of ceria-supported Pd catalysts increases with the interfacial contact between the Pd phase and ceria [6]. Therefore, to maximize this contact, some of us recently used self-assembly methods to synthesize hierarchical, core–shell catalysts, designated here as Pd@CeO_2, that consist of Pd nanoparticles surrounded by a thin porous shell of ceria [7]. These catalysts show remarkable activity for CH_4 combustion under some conditions and offer significant potential to improve the performance of catalysts required to reduce methane emissions. However, despite their high intrinsic activity for methane oxidation, Pd-based catalysts can deactivate under real conditions, especially in the presence of water vapor, sulfur and phosphorus species [8–14].

Phosphorus is a particularly serious poison for CeO_2-promoted catalysts and is a primary agent for irreversible deactivation of automotive catalytic converters under real operating conditions [15–17]. The presence of phosphorus compounds (P_2O_5 or H_3PO_4) in vehicle exhaust is due to decomposition/volatilization of motor oil anti-wear additives, such as zinc dialkyldithiophosphate (ZDDP) [18,19]. These additives are present in most available motor oils in concentration up to 1–2% (although this can vary depending on

* Corresponding author. Fax: +39 405583903.
E-mail address: pfornasiero@units.it (P. Fornasiero).

http://dx.doi.org/10.1016/j.apcatb.2015.10.001
0926-3373/

the final application) and their effect on catalytic converters is well documented [15–17]. Based on studies of simplified, model systems (CeO_2 and $Ce_xZr_{1-x}O_2$) [18–25], it is known that mixed phosphates (Zn, Ca and Mg) form glassy overlayers on the washcoat surface and also react with the catalyst to form $CePO_4$ and $AlPO_4$ [25].

$CePO_4$ formation is irreversible and detrimental to the catalytic activity due to loss of oxygen storage capacity (OSC), which is caused by locking of the Ce^{3+}/Ce^{4+} pair in the 3+ state [24,25]. Both the direct reaction of CeO_2 with phosphorus compounds in the gas phase and the reaction of CeO_2 with P-containing species on the catalyst (*e.g.* aluminum phosphate) can lead to the formation of $CePO_4$ [22]. Based on evidence from total reflection X-ray fluorescence (TXRF), XPS and ^{31}P NMR data on P-poisoned CeO_2, phosphate species formed on the surface and sub-surface region dramatically decrease OSC. Cerium phosphate is also very stable and cannot be removed from either pure CeO_2 or $Ce_xZr_{1-x}O_2$ by calcination treatments to 1000 °C [21,26]. A few studies indicated partial removal of phosphate species by washing the spent catalyst with oxalic acid [18] or chlorine containing species [27]. However, $CePO_4$ persists even after these treatments [18], implying that alternative methods need to be developed to address the problem of P-poisoning.

Despite previous work on regenerating P-poisoned catalysts, relatively little is known about the conditions in which $CePO_4$ is formed. In studies regarding commercial catalysts, the effect of P-aging is evaluated by comparing fresh samples and samples aged for 30,000–160,000 km in conventional automobiles [15–17]. In model systems studies the aging treatment is typically simulated by depositing phosphates by impregnation of the catalyst with $NH_4H_2PO_4$ solutions followed by calcination to get a final P content of 0.04–4.5 wt% [19,21,23]. In one study, CeO_2 aging was performed for only 10 h by introducing 85 ppm H_3PO_4 through the gas feed [22]. Notably, aging effects were similar in model systems and real catalysts, even if the chosen conditions, the materials studied and method of P addition were different. This suggests that model systems studies are relevant to real applications, and also that aging can be very fast as soon as phosphates reach the catalytic bed at a certain temperature of formation. Despite this, to our best knowledge, time-on-stream deactivation studies on commercial or model systems are still too limited. Also, the temperature threshold at which $CePO_4$ is formed was only reported by Xu et al. [22] for pure CeO_2 under lean conditions (600 °C). However, in their study, gas-phase P_2O_5 was introduced by thermal decomposition of aqueous H_3PO_4, resulting in 5% H_2O in the reaction atmosphere. In the present study, we show that the introduction of H_2O in methane combustion reaction mixture enhances the effect of phosphorus poisoning, leading to deactivation. This is particularly relevant to lean-burn engines converters and other real applications, in which water is typically present in 5–15% vol concentration [13,14].

2. Experimental method

2.1. Catalyst synthesis

Potassium tetrachloropalladate(II) (99.95%) and palladium nitrate (99.95%) were purchased from ChemPUR. Cerium ammonium nitrate (CAN, 99.99%), sodium methoxide (25% in methanol), phosphoric acid (85%), 11-mercaptoundecanoic acid (MUA, 95%), dodecanoic acid (99%), triethoxy(octyl) silane (TEOOS, 97.5%), and all the solvents (analytical grade) were obtained from Sigma–Aldrich. Sodium borohydride (98%+) was purchased from Acros Organics. Graphite foils, 0.25 mm thick, were purchased from Alfa Aesar (99.8%, phosphorus-free graphite) and ChemPUR (99%, graphite containing phosphorus). The foils were cut into 9 × 9 mm slides and washed with water and acetone prior to use.

The supramolecular Pd@CeO_2 units were prepared according to published procedures [28]. Briefly, pre-formed Pd nanoparticles protected by 11-mercaptoundecanoic acid (MUA) were mixed with Ce(IV) tetradecyl alkoxide to obtain a Pd:Ce molar ratio of 3.70, leading to the formation of self-assembled units with an intimate Pd–Ce contact. A controlled hydrolysis in the presence of dodecanoic acid leads to the formation of the Pd@CeO_2 structures, in which small crystallites (~3 nm) of CeO_2 organize around the preformed metal particles. These units were deposited from solution onto the two types of graphite, one containing phosphates (P-graphite) and one pure (graphite), according to a procedure described in detail elsewhere [30]. The Pd@CeO_2 batch was diluted 1:10 and the resulting solution was added to the slide 5 times, 0.1 mL at a time, allowing the slide to dry between additions. The Pd@CeO_2/P-graphite and Pd@CeO_2-graphite model catalysts were calcined to 450 °C in air for 5 h. These samples will be referred to as "fresh".

2.2. Aging treatments

Aging treatments were performed in a U-shaped quartz reactor, using an alumina tray to hold the model-catalyst slides in place. Reactions were carried out at a total gas pressure of 1 atm, with the inlet composition controlled by varying the flow rates of CH_4, O_2 and Ar, while maintaining the total flow rate at 21.3 mL min^{-1}. The Gas Hourly Space Velocity (GHSV) was 10^6 mL g^{-1} h^{-1}, using the volume of Pd@CeO_2 dispersion added to the graphite slides.

The heating and cooling rates in all heating measurements were fixed at 10 °C min^{-1}. For experiments that included water, the premixed, gaseous reactant mixture was bubbled through a saturator heated to the temperature required for the desired water feed concentration. The composition of the effluent gases was monitored on-line using a mass spectrometer. At the end of the aging treatment, the system was purged with Ar, cooled to room temperature, and finally stored under Ar until rapid transfer to the XPS chamber.

2.3. Characterization techniques

The X-ray Photoelectron Spectroscopy (XPS) and Synchrotron Radiation Photoelectron Spectroscopy (SRPES) experiments were carried out at the Materials Science Beamline (MSB) at the Elettra Synchrotron Light Source in Trieste, Italy. The MSB is a bending magnet beamline with a plane grating monochromator that provides light in the energy range of 21–1000 eV. The UHV endstation, with a base pressure of 1×10^{-8} Pa, is equipped with an electron energy analyzer (Specs Phoibos 150) and a dual Mg/Al X-ray source. High-resolution, SRPES measurements were performed on the following core levels (photon energies in parentheses): O 1s (610 eV), Pd 3d (610 eV), C 1s (425 eV), and P 2p (425 eV). Complementary XPS spectra of Ce 3d, O 1s, C 1s, P 2p, and Pd 3d core levels were recorded at the same end station using the excitation energy of 1486.6 eV (Al Kα). The apparent degree of reduction of ceria was determined from the Ce 3d spectra using the procedure described in a previous publication [29]. Binding energies are reported after correction for charging using the graphite C 1s as a reference.

Sample surfaces were also examined by means of a field-emission Scanning Electron Microscope (SEM) (Model Tescan Mira 3). High resolution was achieved using an acceleration voltage of 30 kV and a working distance of less than 3 mm. Additionally, a Bruker XFlash® 6 | 10 Energy Dispersive Spectrometer (EDS), mounted on the SEM apparatus, was used to carry out element mapping of the sample. Characteristic X-ray radiation was excited by 20 keV primary electrons.

Atomic Force Microscopy (AFM) was performed using a Nanoscope V (Digital Instruments Metrology Group, model MMAFMLN), in tapping mode in air at room temperature, using

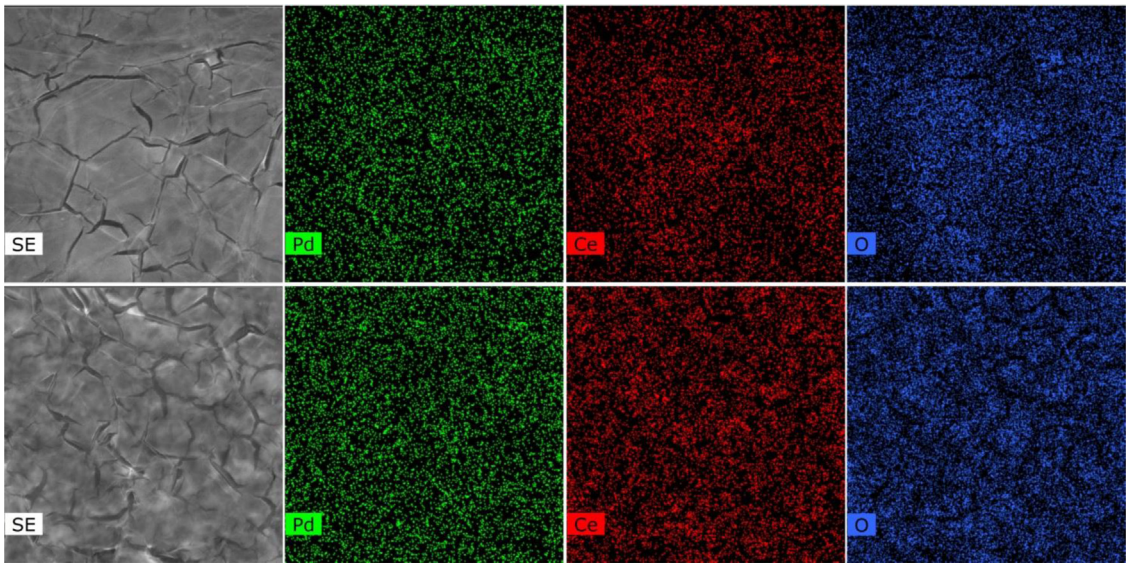

Fig. 1. 20 μm viewfield SEM images and EDS mapping of Pd, Ce and O signals of fresh Pd@CeO_2/graphite (top row) and Pd@CeO_2/P-graphite (bottom row) samples.

an n-type silicon μmash® SPM probe (HQ:NSC15/AL BS) with tip height of 12–18 μm and cone angle < 40° (Resonant frequency 325 kHz, force constant of ~40N/m).

X-ray Absorption Near Edge Structure (XANES) experiments were performed at the SAMBA beamline at Synchrotron SOLEIL (France) with a Si (2 2 0) double crystal monochromator. The monochromator was kept fully tuned and harmonics were rejected by a pair of Pd-coated, Si mirrors. Spectra were recorded in fluorescence mode at the Pd K edge (E = 24350 eV) and Ce L_{III} edge (E = 5723.4 eV) using a 35-element Ge detector. *Operando* experiments were conducted using the transmission and fluorescence cell described elsewhere [30]. Three slides of Pd@CeO_2/P-graphite catalyst and a total gas flow rate of 12 mL min^{-1} (0.5% CH_4, 2.0% O_2, 15.0% H_2O if appropriate, and N_2 balance) were used for both Ce L_{III} edge experiments and Pd K edge experiments. Product analysis was carried out using a Cirrus-MKS mass spectrometer. The observed activity was comparable to that observed during catalytic testing. The fractions of Ce^{3+} and Pd^0 in the samples were determined by fitting the XANES part of the spectrum using a linear combination of spectra for $CePO_4$ and CeO_2 to fit data for Ce and a combination of spectra for PdO and a Pd foil to fit data for Pd. All measurements were performed during the same beam session.

3. Results

The graphitic supports used in this study were analyzed by EDS to determine their P content. As expected, no P was observed on the pure graphite support, while the P-graphite samples contained 1000 ± 100 ppm of P. The P signal did not change appreciably upon deposition of Pd@CeO_2 particles, nor was it affected by any of the aging treatments performed in this study. Complementary XPS/SRPES analysis was performed on the as-received graphitic supports to determine the chemical state of phosphorus and the surface/bulk distribution. Prior to calcination, there was no P signal on either the P-graphite or the pure graphite. A phosphorus signal, at a Binding Energy (BE) corresponding to that of PO_4^{3-} (133 eV) was only observed on the P-graphite after thermal treatment to 450 °C in air (see Fig. S1). Similar treatment of the pure graphite did not cause the appearance of a P signal. This suggests that P is initially present only in the bulk of the P-graphite support and is released during the thermal treatment. An O 1s signal at 530.5 eV appeared together with the P signal, indicating the presence of PO_4^{3-} species. This fingerprint of PO_4^{3-} was present on all Pd@CeO_2/P-graphite samples, independent of aging conditions and with a similar intensity as was observed following calcination at 450 °C. In accordance with these observations, phosphates can be present as intercalating compounds of graphite foils manufactured by squeezing exfoliated graphite [31].

SEM images of the fresh Pd@CeO_2/graphite and Pd@CeO_2/P-graphite catalysts are shown in Fig. 1 and exhibit very similar surfaces, displaying large, smooth domains of a continuous film, separated by small, shallow cracks. The distributions of Pd, Ce and O signals over the samples were homogeneous, demonstrating that the Pd@CeO_2 particles were well-dispersed and exposed to the gas phase for both supports, an important prerequisite for model catalytic systems.

The "fresh" catalysts were then aged for 0 min, 30 min, 1 h, or 9 h under catalytic reaction conditions, at 500 °C and 600 °C, in dry and wet conditions. In all experiments, the catalyst was ramped to the desired temperature in 0.5% CH_4, 2.0% O_2 and 15.0% H_2O (for wet conditions) and held at that temperature for the chosen time span. After aging, the gas flow was switched to pure Ar and the samples cooled to room temperature before being transferred to either the SRPES/XPS line or to the SEM.

As shown in Fig. 2A, the fresh model Pd@CeO_2/graphite catalyst showed significant and constant evolution of CO_2 as result of CH_4 oxidation at both 500 and 600 °C. While rates were stable under dry conditions, the rate of CO_2 production decreased with time at both temperatures when water was added. The Pd@CeO_2/P-graphite samples were less active for methane oxidation (Fig. 2B). Most notably, there was a fast and irreversible deactivation during wet aging at 600 °C. After 1 h of isothermal treatment under these conditions, the sample was almost completely inactive.

SEM images of the aged samples in Fig. 3 show differences between the catalysts supported on graphite and P-containing graphite. The surfaces of the Pd@CeO_2/graphite samples were not appreciably altered by any of the aging treatments. However, images of the Pd@CeO_2/P-graphite samples show features having diameters of 10–30 nm, with sizes that are slightly bigger for 600 °C aging treatments. These spots are partially sintered Pd@CeO_2 particles. The SEM analysis suggests that the presence of phosphorus causes partial aggregation of the Pd@CeO_2 units and growth of crystallite sizes that does not occur in the absence of P.

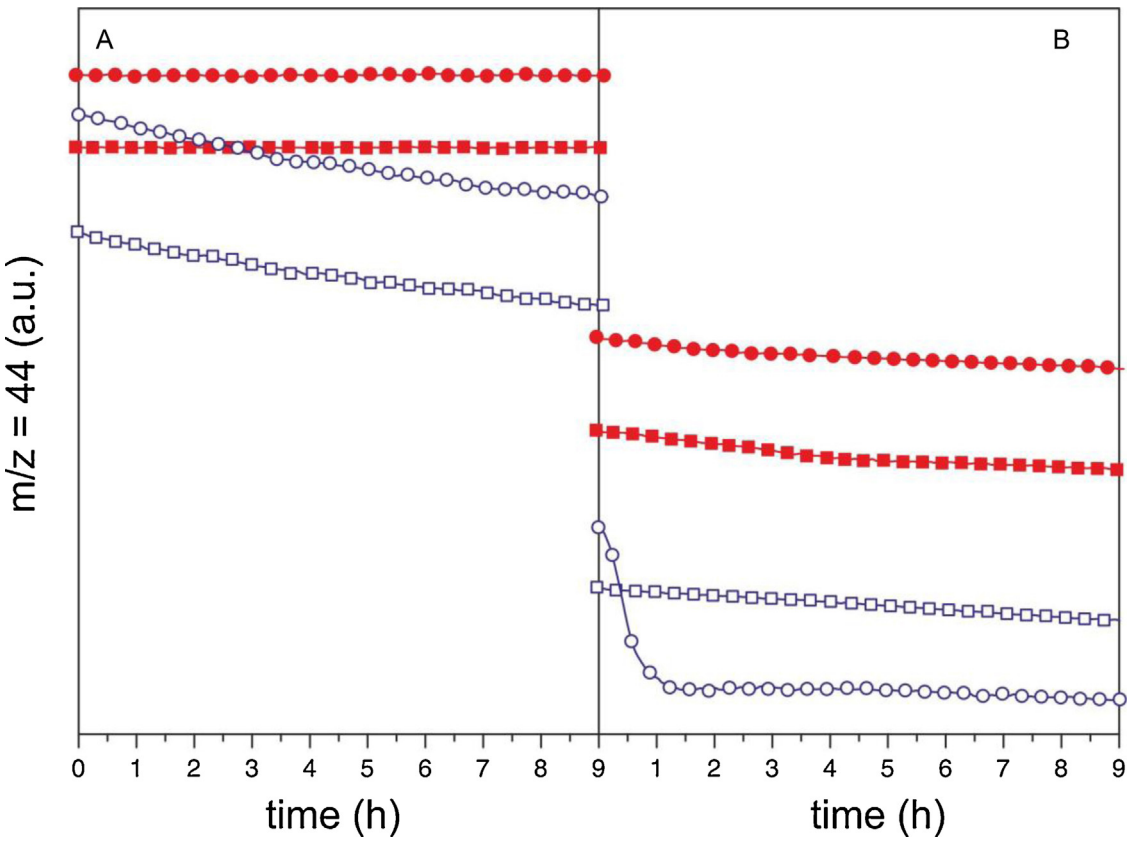

Fig. 2. CO_2 evolution over time. (A) Pd@CeO_2/graphite; (B) Pd@CeO_2/P-graphite. Circles: 600 °C aging; squares: 500 °C aging; filled symbols: dry conditions (CH_4 0.5%, O_2 2%, GHSV: 10^6 mL g^{-1} h^{-1}); open symbols: wet conditions (15% H_2O vapor added to reaction atmosphere).

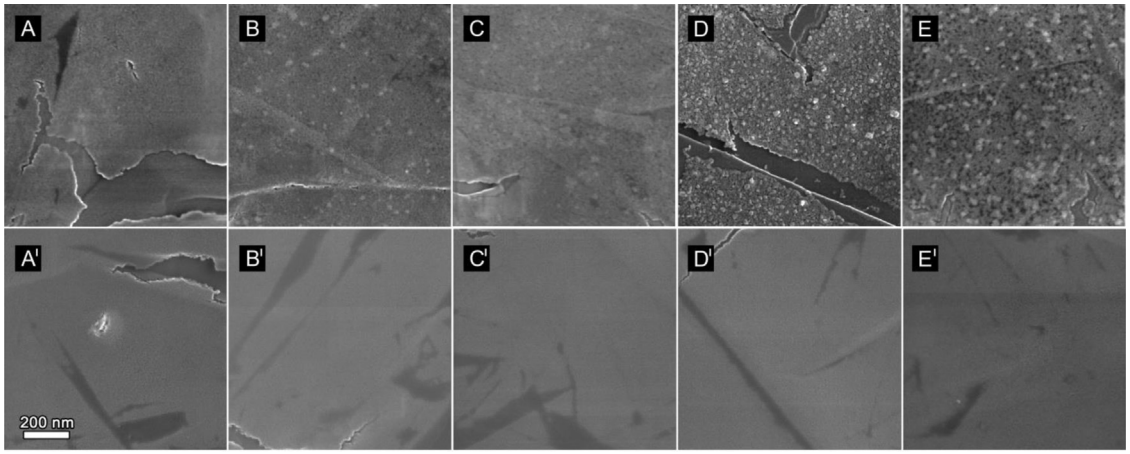

Fig. 3. SEM of Pd@CeO_2/P-graphite (A–E) and Pd@CeO_2/graphite samples (A′–E′). The samples were fresh (A, A′) or treated for 9 h under the following conditions: dry reaction conditions at 500 °C (B, B′) or 600 °C (D, D′); wet reaction conditions at 500 °C (C, C′) and 600 °C (E, E').

Fig. 4 indicates that the Ce 3d region of the XPS spectra is very different for the Pd@CeO_2/graphite and Pd@CeO_2/P-graphite samples. Spectra on the Pd@CeO_2/graphite samples were all similar, with features typical of pure CeO_2. Initially, the apparent O:Ce stoichiometry is 1.94 (12% Ce^{3+}) but it increases to 2.0 with aging time. Apparently, a small fraction of the cerium is in the Ce^{3+} state in the initial particles but all of the Ce atoms are converted to Ce^{4+} under the aging conditions used in this study. This behavior differs from that observed for Pd@CeO_2/Si-Al_2O_3 catalysts, which showed a low but constant Ce^{3+} fraction for all the treatments [13]. Various factors could contribute to this, including the different surface sensitivity of the techniques used (XPS-XAS) and the different Pd:Ce ratio, but the different calcination temperatures used here (450 °C *vs* 850 °C) and the different supports (Al_2O_3 *vs* graphite) are likely the primary causes. On the Pd@CeO_2/P-graphite sample, in contrast, the XPS spectra show mainly features of $CePO_4$ [19,32], even on the fresh sample, for which Ce^{4+} is also still observed. Spectra taken after heating to 500 °C under dry and wet aging were similar to each other and showed only small changes compared to the fresh sample. On the other hand, aging treatments at 600 °C resulted in dramatic changes. After 30 min of wet aging at this temperature, the Ce^{4+} signal completely disappeared. Spectra obtained after prolonged dry aging (9 h) showed partial oxidation to Ce^{4+} with respect to the fresh sample.

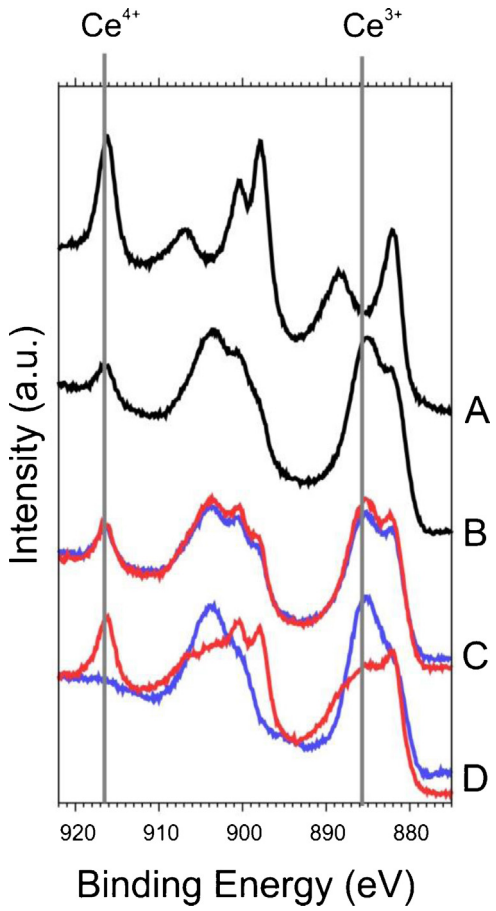

Fig. 4. Representative Ce 3d XPS spectra of: (A) the fresh Pd@CeO_2/graphite sample; (B) fresh Pd@CeO_2/P-graphite; (C) Pd@CeO_2/P-graphite aged at 500 °C; (D) Pd@CeO_2/P-graphite aged at 600 °C. Dry conditions are shown by red lines and wet conditions by the blue lines. The areas of the presented spectra have been normalized after subtraction of Shirley background and the curves have been offset for clarity. The positions of the most prominent peaks in Ce^{4+} and Ce^{3+} spectra are marked by grey lines. (For interpretation of the references to color in this figure legend, the reader is referred to the web version of this article.)

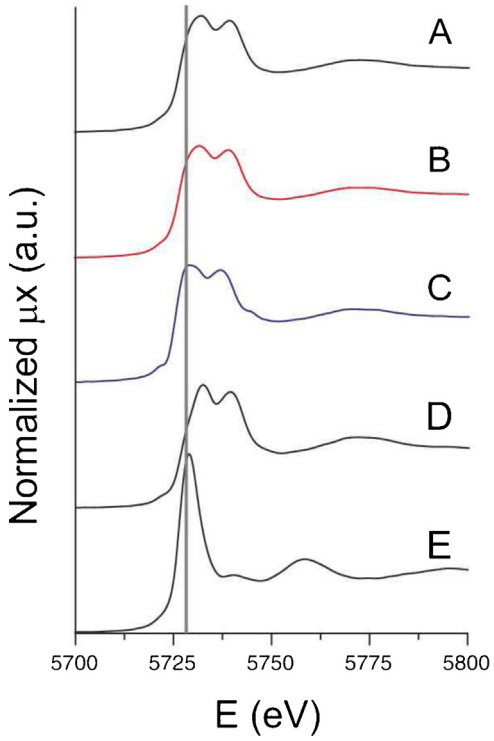

Fig. 6. *Operando* XANES spectra of Pd@CeO_2/P-graphite sample at Ce L_{III} edge: (A) fresh; (B) during dry aging at 600 °C; (C) during wet aging at 600 °C. Reference spectra: CeO_2 (D), $CePO_4$ (E).

Fig. 5 shows the percentage of Ce^{3+} on the Pd@CeO_2/P-graphite sample for the different aging conditions. Since, in the absence of P, the Ce in the Pd@CeO_2 particles is almost completely oxidized to Ce^{4+} after the initial calcination and after all aging treatments, the trends observed for the Ce^{3+} percentage in this case are indicative of $CePO_4$ formation on the surface of the particles sampled by XPS. The fresh sample contains 75% Ce^{3+}, demonstrating that the particles are extensively covered by $CePO_4$ already after calcination. For aging at 500 °C, the percentage of Ce^{3+} does not change appreciably, regardless of the aging conditions (dry or wet). However, aging at 600 °C changed the sample dramatically. Wet aging caused an increase in Ce^{3+} percentage to 100% after 30 min, while dry aging decreased the Ce^{3+} content, to 40% Ce^{3+} after

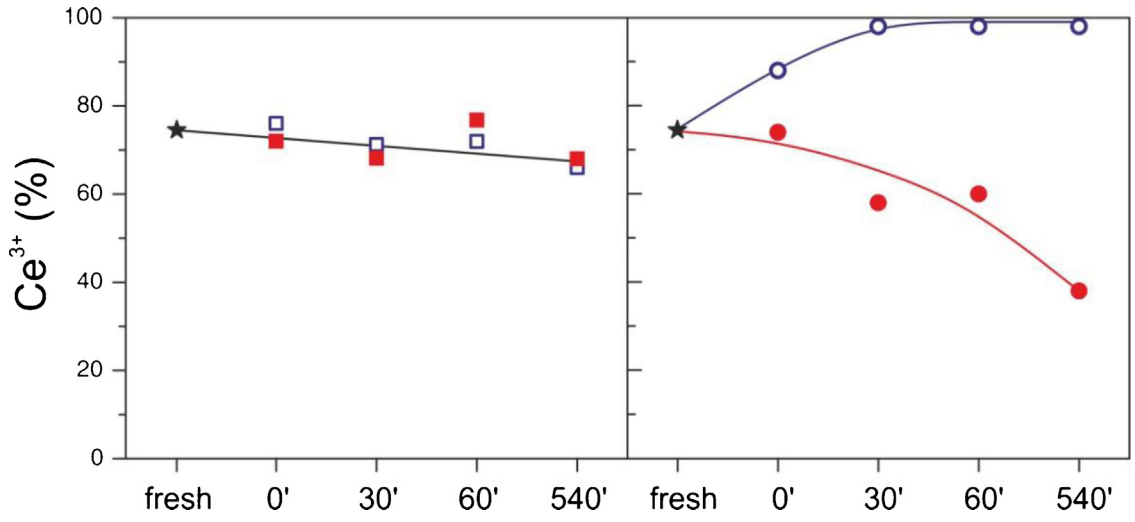

Fig. 5. Calculated $Ce3^+$ percentage for Pd@CeO_2/P-graphite samples, determined by fitting of Ce 3d XPS spectra. Fresh samples: star. Squares: aged at 500 °C (filled: dry conditions, empty: wet conditions). Circles: aged at 600 °C (filled: dry conditions, empty: wet conditions). The solid lines are guides to the eye.

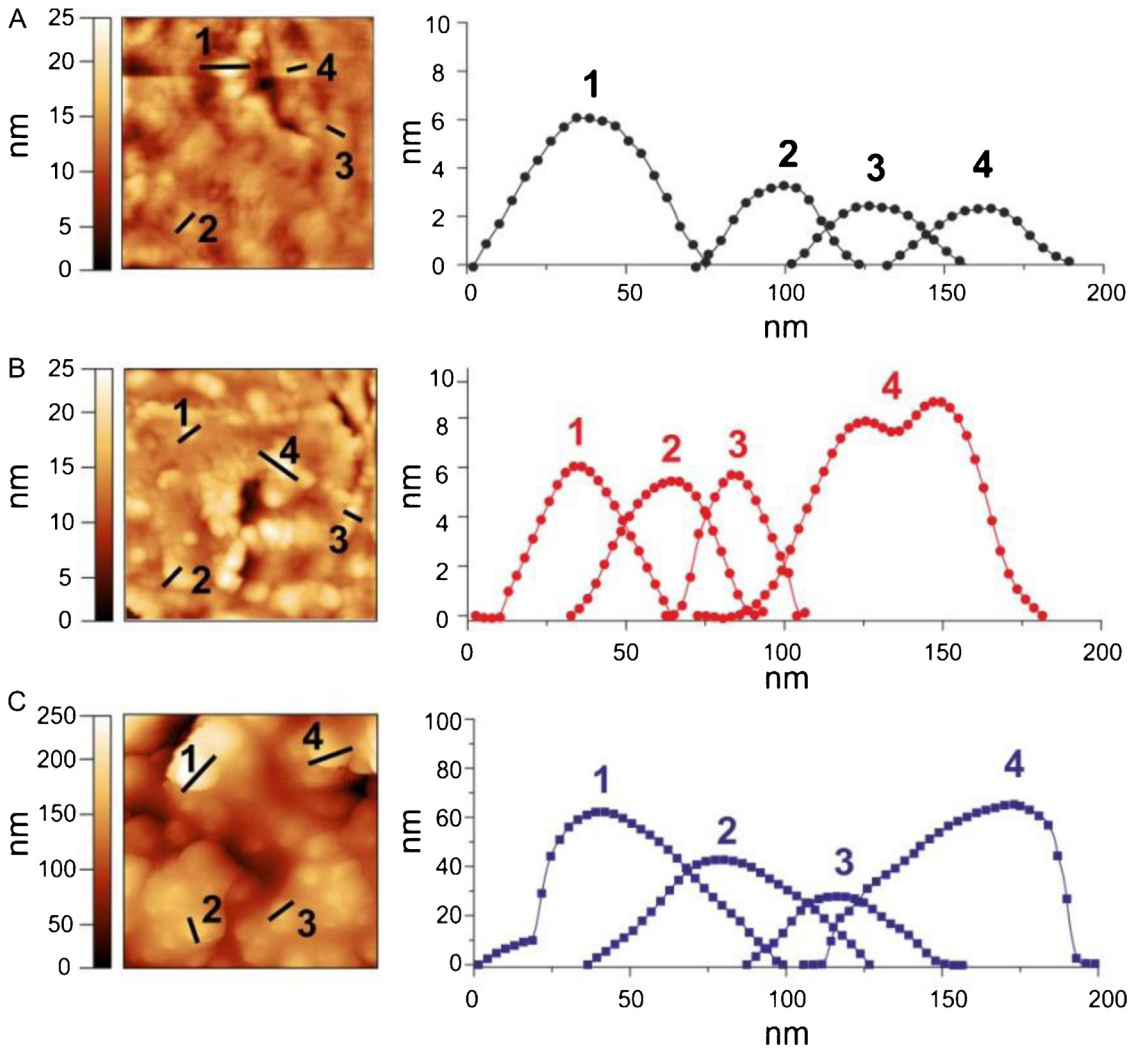

Fig. 7. AFM topography images with representative line scans for Pd@CeO_2/P-graphite: (A) fresh; (B) aged at 600 °C under dry conditions for 9 h; (C) aged under wet conditions at 600 °C for 9 h. Please note the different scales in part C.

9 h. These results indicate a crucial role for water in the formation, accumulation, and stabilization of phosphates on ceria.

To gain further insights into the extent of $CePO_4$ formation and the extent of cerium reduction, *operando* and *ex-situ* XANES measurements were performed on the Pd@CeO_2/P-graphite catalysts, with representative results shown in Fig. 6. In all cases, only minor differences were observed between fresh, dry-aged and wet-aged samples, at both 500 °C and 600 °C. In contrast to the XPS results, the Ce^{3+} percentage did not evolve during aging treatments and ranged from 15% to 18% in all the samples studied. Indeed, these results are similar to recent *in-situ* EXAFS data on a Pd@CeO_2/Si-Al_2O_3 powder having a similar Pd@CeO_2 composition with no P poisoning. That study also indicated the presence of 20% Ce^{3+} in the fresh catalyst [13].

The dramatic difference in the valence ratios calculated from XPS and XANES implies that the surface and bulk concentrations can be very different on these samples. Since the inelastic mean free path in CeO_2 of the photoelectrons originating from Ce 3d level in the XPS study is approximately 1.2 nm and the expected dimensions of the CeO_2 crystallites in the Pd@CeO_2 particles is 3–4 nm [6,30], the large difference between surface and bulk concentrations cannot be explained by the presence of $CePO_4$ at the surface of the initial Pd@CeO_2 core–shell particles. Rather, the data indicate that thermal sintering or partial aggregation of ceria crystallites must occur under wet aging at 600 °C.

To further investigate the evolution of the Pd@CeO_2 particles dimensions during aging, the Pd@CeO_2/graphite and Pd@CeO_2/P-graphite samples were characterized by AFM topographic analysis. Fig. 7 shows images and height profiles for the Pd@CeO_2/P-graphite sample, both fresh and after 9-h aging at 600 °C. Results for the Pd@CeO_2/graphite sample are not shown but were essentially identical to that observed for fresh Pd@CeO_2/P-graphite, even with various aging treatments. For both Pd@CeO_2/graphite and Pd@CeO_2/P-graphite, the fresh and dry aged samples showed small features, approximately 10 nm in height, similar to what was observed for Pd@CeO_2 particles deposited onto YSZ(1 0 0) single crystals [33] (Fig. 7A and B). Wet aging did not appreciably change the Pd@CeO_2/graphite sample at either 500 °C or 600 °C. However, wet aging at 600 °C caused dramatic sintering on the Pd@CeO_2/P-graphite sample, leading to the appearance of features that were 50–60 nm high and 50–70 nm wide, distributed over a corrugated surface (Fig. 7C). The changes in particle size help explain how the bulk and surface compositions can be so different.

Fig. 8 shows XPS/SRPES spectra for the O 1s region of the Pd@CeO_2/graphite and Pd@CeO_2/P-graphite samples and the results support the conclusions reached from the Ce 3d core level. The spectrum of the fresh Pd@CeO_2/graphite sample, Fig. 8A, shows two peaks at 529.2 eV and 531.6 eV. The peak at lower BE can be assigned to bulk CeO_2, while the higher BE peak is likely due to hydroxyl species [34]. However, the presence of

other species having similar BE cannot be entirely ruled out. Carbonates arising from reaction with the graphite supports are not expected to form during the thermal treatments performed here; also, similar O 1s spectra were observed for Pd@CeO_2 on Au (not reported here). When the Pd@CeO_2/graphite sample was aged under wet conditions, Fig. S2, the intensity of the peak at 532 eV was enhanced and a slight shift to higher binding energies was observed, further supporting the assignment of the signal to hydroxyl species [9,13,34]. With Pd@CeO_2/P-graphite, the spectrum of the fresh sample, Fig. 8B, again showed a peak near 529 eV due to bulk CeO_2 but the largest peak was centered at 530.4 eV, which can be assigned to $CePO_4$ based on the preliminary analysis performed on the P-containing graphite. There was very little change in the spectrum of samples aged under dry conditions at either 500 °C or 600 °C, but wet aging at either temperature gave increased intensity in the region assigned to hydroxyls. After wet aging at 600 °C, the peak associated with bulk CeO_2 essentially disappeared. This is consistent with the disappearance of the Ce^{4+} signal in the Ce 3d region of the 600 °C wet-aged samples.

XPS spectra of the Pd 3d region on representative samples are shown in Fig. 9. For both Pd@CeO_2/graphite and Pd@CeO_2/P-graphite, the fresh samples show two peaks at 337.2 eV and 342.4 eV, which are almost certainly due to PdO. The two peaks are due to the Pd spin–orbit split doublet (Pd $3d_{5/2}$ and Pd $3d_{3/2}$). The BE of the doublet is actually close to the BE expected for PdO_2 [35]; however, a shift to higher binding energy is often observed for metal and metal–oxide nanoparticles, including Pd and PdO [36–42]. For example, the $3d_{5/2}$ signals of both PdO and Pd nanoparticles have previously been reported to shift to approximately 1.0 eV higher BE due final-state effects [36,40]. The fact that our samples contained PdO was confirmed by *operando* and *ex-situ* XANES measurements on both the graphite and P-graphite supported catalysts (Fig. S4).

Neither wet nor dry aging had any effect on the XPS spectrum for Pd on the Pd@CeO_2/graphite sample; however, the same was not true for Pd@CeO_2/P-graphite. While dry aging did not affect the spectrum, wet aging of the P-containing sample at 600 °C resulted in the complete disappearance of the Pd signal. Since EDS and XANES results demonstrate that Pd is not lost under these conditions (Fig. S4), the loss of Pd signal in XPS must be due to burial of Pd under the $CePO_4$. This agrees with the SEM results, showing that the Pd@CeO_2 particles undergo severe sintering during wet aging when P is present.

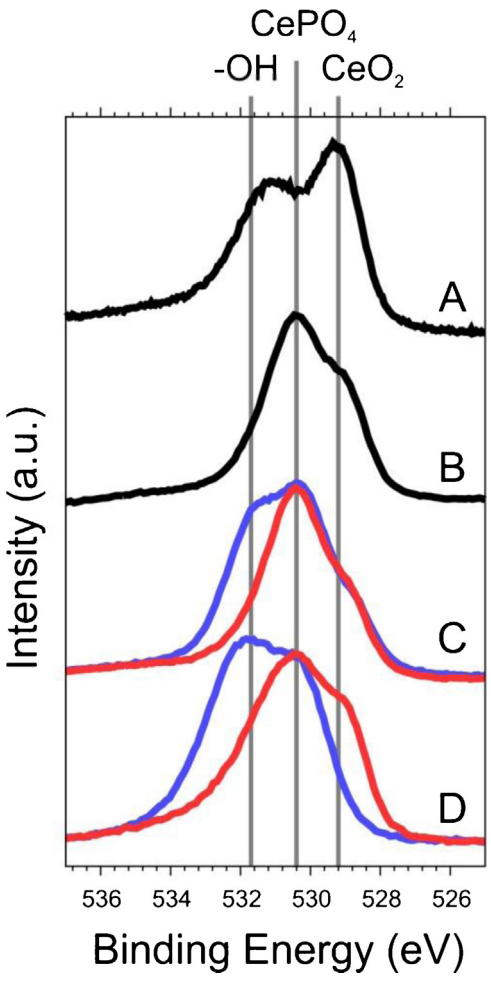

Fig. 8. Representative O 1s XPS spectra: (A) fresh Pd@CeO_2/graphite; (B) fresh Pd@CeO_2/P-graphite; (C) Pd@CeO_2/P-graphite aged at 500 °C; (D) Pd@CeO_2/P-graphite aged at 600 °C. The red lines were obtained after aging under dry conditions and the blue lines under wet conditions. The areas of the presented spectra have been normalized to the $CePO_4$ contribution (B–D) and the P free sample (A) has been adjusted to comparable intensity. The curves have been offset for clarity. The positions of assigned O 1s contributions are marked with grey lines. (For interpretation of the references to color in this figure legend, the reader is referred to the web version of this article.)

4. Discussion

One of the main objectives of this work was to study the effect of P-poisoning on the catalytic performance of Pd-CeO_2 catalysts. Similarly to other P-poisoning studies, phosphorus was deliberately introduced in the system during the catalyst preparation [19,21,23], rather than introducing it from the gas feed during aging treatments [22]. In this way, H_2O is not introduced in the reaction mixture by decomposition of H_3PO_4 to P_2O_5 and the effect of water addition can be studied separately. The combined results in this study demonstrate that the presence of phosphorus in the vicinity of a Pd/ceria catalyst results in the rapid formation of $CePO_4$ at temperature as low as 450 °C. Since vapor pressure of phosphates is negligible under these conditions, the formation of $CePO_4$ indicates that there is a high affinity of Ce and P. This agrees with previous results from Xu et al., who observed formation of $CePO_4$ from the reaction of CeO_2 with $AlPO_4$ [22]. Notably, the distribution of $CePO_4$ in the surface and subsurface of CeO_2 particles is in agreement with other observations from the literature [19,22–25], even if the source of phosphorus and aging conditions were different.

Interestingly, the phosphorous-poisoned catalysts maintain a relatively high activity under dry conditions, despite being extensively covered by phosphates. Indeed, the XPS spectra even indicate that cerium phosphate can be partially removed from the surface of ceria particles at 600 °C under dry conditions. In agreement with this, López Granados et al. reported that, on P-poisoning of CeO_2 by addition of $(NH_4)_2HPO_4$, followed by calcination to 600 °C [19] some of the CeO_2 surface was not converted to $CePO_4$ and was still available for oxygen exchange with gas-phase oxygen, even for samples having a high P:Ce ratio.

The presence of water changes things completely, and a rapid, irreversible deactivation is observed at temperatures above 600 °C. At these temperatures, $CePO_4$ becomes highly mobile and causes severe aggregation of ceria particles and Pd encapsulation. The results of this study indicate that water and phosphorus have a cooperative effect and take part in a deactivation mechanism activated by high temperature. For the first time, the deactivation of Pd-CeO_2 catalysts in the presence of P was studied in steady-state experiments, revealing that poisoning occurs in very short time under conditions relevant for real applications [22,23,25]. Although surface blockage by $CePO_4$ is reported in the literature as the main effect of P-poisoning on ceria-based catalysts, our work reveals that phosphorus can

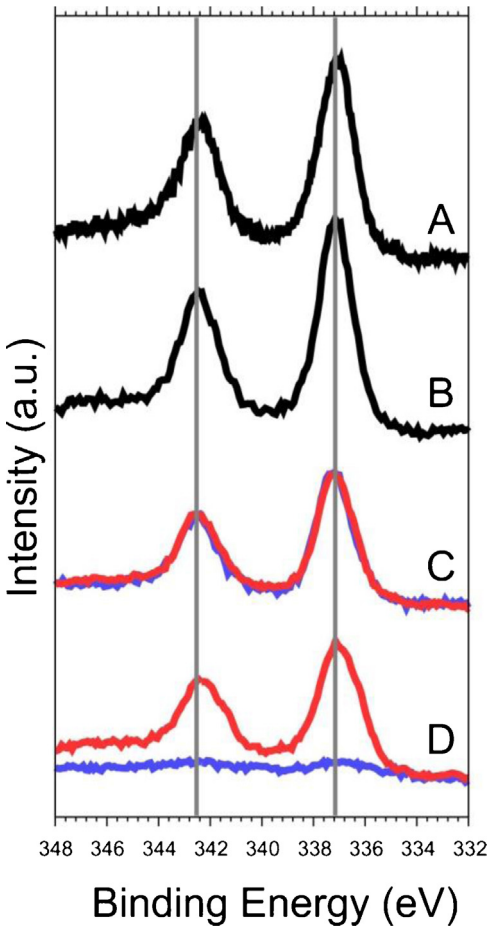

Fig. 9. Representative Pd 3d XPS spectra: (A) Pd@CeO_2/graphite; (B) fresh Pd@CeO_2/P-graphite; (C) Pd@CeO_2/P-graphite aged at 500 °C; (D) Pd@CeO_2/P-graphite aged at 600 °C. Aging under dry conditions is indicated by the red lines while wet aging is indicated in blue. The curves have been offset for clarity. (For interpretation of the references to color in this figure legend, the reader is referred to the web version of this article.)

also cause deep morphological transformations of the catalyst and dramatic loss of activity, especially in the presence of water.

5. Conclusions

The effect of phosphorus poisoning on the catalytic combustion of methane over Pd@CeO_2/graphite catalysts was found to be dramatically influenced by temperature and presence of H_2O. When P was not introduced in the catalyst formulation, the catalysts were active and stable under all studied conditions (500–600 °C; dry and wet conditions). On the other hand, P-poisoned catalysts were less active and stable because of partial thermal sintering. Water vapor causes rapid and complete deactivation at higher temperatures by inducing severe aggregation of ceria nanoparticles, incorporation of Pd active phase in the bulk of the crystallites and exposure of $CePO_4$ to the catalyst surface. The combination of XPS/SRPES, *operando* XANES measurements, SEM/EDS and AFM techniques provides evidence of a temperature dependent, water-driven P-poisoning of Pd and CeO_2-based oxidation catalysts.

Acknowledgements

We acknowledge SOLEIL for provision of synchrotron radiation facilities and we would like to thank V. Briois and G. Alizon for assistance in using beamline SAMBA. Dr. Emiliano Fonda is acknowledged for expert assistance in acquisition and discussion of XANES data. University of Trieste (Project FRA2013), MIUR, Italy (project HI-PHUTURE protocol 2010N3T9M4), COST Action CM1104—Reducible oxide chemistry, structure and functions, European Community (project FP7-NMP-2012-SMALL-6- project ID 310651) and the CERIC SPL-MSB project are acknowledged for financial support. R.J.G. is grateful for support from the Department of Energy, Office of Basic Energy Sciences, Chemical Sciences, Geosciences and Biosciences Division, Grant No. DE-FG02-13ER16380.

Appendix A. Supplementary data

Supplementary data associated with this article can be found, in the online version, at http://dx.doi.org/10.1016/j.apcatb.2015.10.001.

References

[1] D. Ciuparu, M.R. Lyubovsky, E. Altman, L.D. Pfefferle, A. Datye, Catal. Rev. 44 (2002) 593–649.
[2] W.R. Schwartz, L.D. Pfefferle, J. Phys. Chem. C 116 (2012) 8571–8578.
[3] S.K. Matam, G.L. Chiarello, Y. Lu, A. Weidenkaff, D. Ferri, Top. Catal. 56 (2013) 239–242.
[4] S. Colussi, A. Gayen, M.F. Camellone, M. Boaro, J. Llorca, S. Fabris, A. Trovarelli, Angew. Chemie—Int. Ed. 48 (2009) 8481–8484.
[5] S. Colussi, C. De Leitenburg, G. Dolcetti, A. Trovarelli, J. Alloys Compd. 374 (2004) 387–392.
[6] M. Cargnello, V.V.T. Doan-Nguyen, T.R. Gordon, R.E. Diaz, E.A. Stach, R.J. Gorte, P. Fornasiero, C.B. Murray, Science 341 (2013) 771–773.
[7] M. Cargnello, J.J.D. Jaen, J.C.H. Garrido, K. Bakhmutsky, T. Montini, J.J.C. Gamez, R.J. Gorte, P. Fornasiero, Science 337 (2012) 713–717.
[8] D.L. Mowery, R.L. McCormick, Appl. Catal. B Environ. 34 (2001) 287–297.
[9] D. Ciuparu, L. Pfefferle, Appl. Catal. A Gen. 209 (2001) 415–428.
[10] D. Ciuparu, N. Katsikis, L. Pfefferle, Appl. Catal. A Gen. 216 (2001) 209–215.
[11] K. Persson, L.D. Pfefferle, W. Schwartz, A. Ersson, S.G. Järås, Appl. Catal. B Environ. 74 (2007) 242–250.
[12] D. Ciuparu, E. Perkins, L. Pfefferle, Appl. Catal. A Gen. 263 (2004) 145–153.
[13] M. Monai, T. Montini, C. Chen, E. Fonda, R.J. Gorte, P. Fornasiero, ChemCatChem 7 (2015) 2038–2046.
[14] R.J. Farrauto, Science 337 (2012) 659–660.
[15] L. Martín, Appl. Catal. B Environ. 44 (2003) 41–52.
[16] I. Heo, J.W. Choung, P.S. Kim, I.-S. Nam, Y. Il Song, C.B. In, G.K. Yeo, Appl. Catal. B Environ. 92 (2009) 114–125.
[17] C. Larese, Appl. Catal. B Environ. 40 (2003) 305–317.
[18] D. Uy, A.E. O'Neill, L. Xu, W.H. Weber, R.W. McCabe, Appl. Catal. B Environ. 41 (2003) 269–278.
[19] M. Lopez Granados, F. Galisteo, P. Lambrou, R. Mariscal, J. Sanz, I. Sobrados, J. Fierro, A. Efstathiou, J. Catal. 239 (2006) 410–421.
[20] F. Benissad-Aissani, H. Aï̈t-Amar, M.-C. Schouler, P. Gadelle, Carbon 42 (2004) 2163–2168.
[21] C. Larese, M. López Granados, R. Mariscal, J.L.G. Fierro, P.S. Lambrou, A.M. Efstathiou, Appl. Catal. B Environ. 59 (2005) 13–25.
[22] L. Xu, G. Guo, D. Uy, A. O'Neill, W. Weber, M. Rokosz, R. McCabe, Appl. Catal. B Environ. 50 (2004) 113–125.
[23] S.Y. Christou, M.C. Álvarez-Galván, J.L.G. Fierro, A.M. Efstathiou, Appl. Catal. B Environ. 106 (2011) 103–113.
[24] C. Larese, F. Galisteo, M. Granados, R. Mariscal, J. Fierro, P. Lambrou, A. Efstathiou, J. Catal. 226 (2004) 443–456.
[25] S.Y. Christou, S. García-Rodríguez, J.L.G. Fierro, A.M. Efstathiou, Appl. Catal. B Environ. 111–112 (2012) 233–245.
[26] C. Larese, F. Cabello Galisteo, M. López Granados, R. Mariscal López, J.L. Fierro, P. Lambrou, A. Efstathiou, Appl. Catal. B Environ. 48 (2004) 113–123.
[27] S. Christou, A. Efstathiou, Top. Catal. 56 (2013) 255–260.
[28] M. Cargnello, N.L. Wieder, T. Montini, R.J. Gorte, P. Fornasiero, J. Am. Chem. Soc 132 (2010) 1402–1409.
[29] T. Skála, F. Šutara, K.C. Prince, V. Matolín, J. Electron Spectros. Relat. Phenomena 169 (2009) 20–25.
[30] C. La Fontaine, L. Barthe, A. Rochet, V. Briois, Catal. Today 205 (2013) 148–158.
[31] B. Özmen-Monkul, M.M. Lerner, Carbon 48 (2010) 3205–3210.
[32] Y. Zhang, J. Wang, T. Zhang, Chem. Commun. 47 (2011) 5307–5309.
[33] L. Adijanto, D.A. Bennett, C. Chen, A.S. Yu, M. Cargnello, P. Fornasiero, R.J. Gorte, J.M. Vohs, Nano Lett. 13 (2013) 2252–2257.
[34] D.R. Mullins, P.M. Albrecht, T.-L. Chen, F.C. Calaza, M.D. Biegalski, H.M. Christen, S.H. Overbury, J. Phys. Chem. C 116 (2012) 19419–19428.

[35] N. Tsud, V. Johánek, I. Stará, K. Veltruská, V. Matolıín, Surf. Sci. 467 (2000) 169–176.
[36] H. He, C. Gao, Molecules 15 (2010) 4679–4694.
[37] P. Zhang, T.K. Sham, Phys. Rev. Lett. 90 (2003) 245502.
[38] J. Morales, J.P. Espinos, A. Caballero, A.R. Gonzalez-Elipe, J.A. Mejias, J. Phys. Chem. B 109 (2005) 7758–7765.
[39] V. Johánek, I. Stará, N. Tsud, K. Veltruská, V. Matolín, Appl. Surf. Sci. 162 (2000) 679–684.
[40] H.-F. Wang, W.E. Kaden, R. Dowler, M. Sterrer, H.-J. Freund, Phys. Chem. Chem. Phys. 14 (2012) 11525–11533.
[41] S. Penner, P. Bera, S. Pedersen, L.T. Ngo, J.J.W. Harris, C.T. Campbell, J. Phys. Chem. B 110 (2006) 24577–24584.
[42] R. Lin, R.G. Freemantle, N.M. Kelly, T.R. Fielitz, S.O. Obare, R.Y. Ofoli, Nanotechnology 21 (2010) 325605.